The 8th European Congress on Computational Methods in Applied Sciences and Engineering
ECCOMAS Congress 2022
5 – 9 June 2022, Oslo, Norway

ANALYTICAL AND NUMERICAL MODELING OF SHOCK WAVE STRESSES AND SPALL CAUSED BY LASER PLASMA AT A MATERIAL INTERFACE – APPLICATION TO PAINT STRIPPING ON ALUMINUM SUBSTRATES

KOSMAS PAPADOPOULOS, KONSTANTINOS TSERPES

Laboratory of Technology & Strength of Materials (LTSM)
Department of Mechanical Engineering & Aeronautics, University of Patras
Rio, Patras – 26500, Greece
e-mail: kitserpes@upatras.gr, kosmaspapadopoulos@upnet.gr

Key words: Laser shock, Paint stripping, Shock wave propagation, Spall fracture, Finite element analysis

Abstract. In the present work, analytical and numerical models have been developed to calculate shock wave stresses caused by laser plasma in a material interface. The input pressure causing the shock wave has been derived from a laser-matter interaction model. The material velocity, stresses, and strains versus time in the two materials and the interface have been computed by solving the jump equations for conservation of mass and balance of momentum. The material interface has been considered as an immovable boundary while the back free surface as an unrestrained boundary. Spall fracture strength of the interface was evaluated and was used as stripping criterion. The model has been used for the fast computation of interfacial stresses causing paint stripping on aluminium substrates and the subsequent fast assessment of stripping initiation. An explicit finite element model combined with the cohesive zone modelling method and a spall fracture model have been developed. These models have been compared to each other in terms of time, accuracy and input properties demand and to the experimental results.

1 INTRODUCTION

Laser shock applications in materials processing have grown significantly in recent years and can be used for paint stripping of aeronautical and aerospace structures [1], [2]. In conventional paint stripping, hazardous chemicals and media blasting are used, thus damaging the substrate. This brings the need for the development of more sustainable methods, with less environmental impact. A candidate method is the laser shock paint stripping (LSPS). In LSPS, the objective is the removal of the paint without causing any damage on the substrates, which might counterbalance the recycling and reusing processes. The stripping can be expressed as the fracture of the interface between the paint and the substrates. This fracture because of the dynamic nature of the laser shock loading and the high strain rates that take place is examined through the *spall fracture mechanism*.

To optimize the LSPS method, a good understanding of the physical phenomena that take place is needed. Aside to the numerous experimental works, several analytical [3]–[6] models

have been developed to describe the shock wave propagation and its interaction inside a solid material. This is not an easy task due to the nature of the shock wave, which acts as a discontinuity inside the material. Analytical models describe mathematically the shock wave propagation through the *jump equations* which arise from the conservation of mass, the balance of momentum and energy principles, solving thus, the problem of the discontinuity. Fracture mechanics, and especially the spall mechanism [4], [7]–[9], have contributed by describing the failure of materials under high strain rate conditions.

In addition to analytical methods numerical models [1], [2], [10], [11] have been widely used to simulate the mechanical behavior of the material due to shock wave propagation. Finite element (FE) models are capable of detailed stress field prediction. Combining FE models with the cohesive zone modeling (CZM) someone can take the mechanical response of the interface between two materials, which is crucial for the examination of the laser shock stripping application.

In the present paper, we have developed computational tools of decreasing computational effort by combining the dynamic nature of the shock wave with the theory of the spall fracture via analytical and numerical study of the laser shock stripping mechanics, to compute the stress field at the aluminum/interface and to predict the stripping initiation in an aluminum/epoxy specimen.

2 PROBLEM OVERVIEW AND APPROACH

Consider an aluminum plate covered with a layer of epoxy paint [1], [2]. The laser is applied on the aluminum side. In Fig. 1, the different interactions of the propagating shock inside the plate are described. The solid line indicates the elastic precursor, the dashed line the plastic shock and the red line the decompression shock.

1. First the loading is applied to the aluminum free surface by the laser plasma and a shock wave initiates inside the material.
2. The shock wave is separated to an *elastic precursor* that takes the material from state 0 to state 1 and to a *plastic shock* that takes the material to state 2.
3. When the loading is removed from the surface of the aluminum a *decompression elastic – plastic shock* initiates.
4. The elastic part of the compressive shock interacts with the aluminum/epoxy interface and a left propagating compressive shock moves inside the aluminum taking to it to state 3.
5. This left propagating shock interacts with the plastic shock and takes the material from state 3 to state 4.
6. Part of the shock wave starts propagating inside the epoxy material taking it to state 3'.
7. When the shock wave that is propagating inside epoxy meets the free surface it reflects to a left propagating decompression shock taking epoxy to state 4'.
8. The plastic shock then reflects from the interface and takes the aluminum from state 4 to state 5, while part of it propagates inside the epoxy, taking it to state 5' and reflects from the free surface to a decompression shock that takes the epoxy to state 6'.

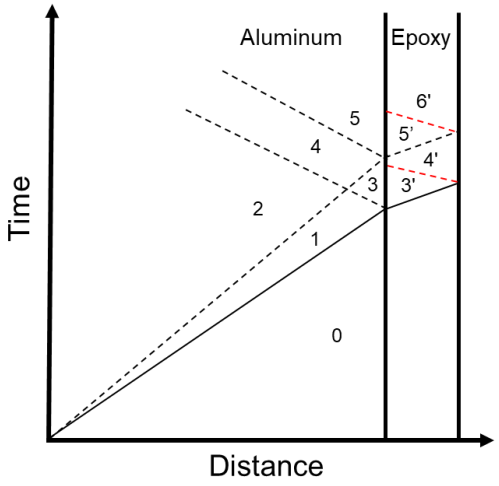

Figure 1: Schematic representation of the shock wave propagation inside aluminum/epoxy material [12]

Using this generated shock wave the paint removal is achieved through the propagation of state 4' and 6' to the interface. The stripping can be distinguished in two main domains: the failure of the paint and the fracture of the interface between paint and the substrate. It is worth mentioning that in the present work the stripping by the laser shock is examined as a pure mechanical process without considering any thermal effects.

3 ANALYTICAL MODELING OF THE STRESS FIELD

A shock wave is a propagating surface at which the displacement is continuous but the mass density, the particle velocity, the stress, and other field variables are discontinuous. For the characterization of plane shocks embedded in smooth uniaxial motion, the following jump conditions were developed [3]

Conservation of mass: $$\rho_R U_s \; -v \; = \; \dot{x} \tag{1}$$

Balance of momentum: $$\rho_R U_s \; \dot{x} \; = \; -t_{11} \tag{2}$$

Balance of energy: $$\rho_R U_s \left[\!\!\left[\varepsilon + \frac{1}{2}\dot{x}^2 \right]\!\!\right] = \; -t_{11}\dot{x} \tag{3}$$

where ρ is the material's density, U_s is the shock velocity, $\dot{x}$ is the material's velocity, t_{11} is the Cauchy stress, v is the specific volume and ε is the specific internal energy. Some further assumptions and considerations must be made before reaching to the analytical solution. The medium is considered as a homogenous and isotropic elastic-plastic material that is subjected to small uniaxial deformation. Also, the analysis is restricted to weak shocks so the thermal variables can be neglected.

The compression shock waves are produced by a sudden application of a uniform compressive load. While the shock has a compressive amplitude lower than the *Hugoniot Elastic Limit* (HEL), it involves only the elastic response. A shock of greater amplitude than the HEL is unstable, and it separates in two shocks, the elastic precursor that propagates at the elastic wave speed C_0 and the plastic shock that propagates at the bulk wave speed C_B, given by the following equations

Elastic wave speed $$C_0 = \sqrt{\frac{\lambda_R + 2\mu_R}{\rho_R}} \tag{4}$$

Bulk wave speed $$C_B = \sqrt{\frac{\lambda_R + \left(2/3\right)\mu_R}{\rho_R}} \tag{5}$$

where $\lambda_R = \frac{E\nu}{(1+\nu)(1-2\nu)}$ and $\mu_R = G$ are the first and second Lame parameters, respectively, where E is the Young's modulus, ν is the Poisson's ratio and G is the shear modulus.

Last, it is important to mention the two types of reflection surfaces and how the shock interacts with them. The reflection from an unrestrained boundary acts like an interface with an incompressible body and the shock that is reflected is compressive. The shock that is reflected from an unrestrained boundary is a decompression wave.

The correlation between the laser's intensity and the applied pressure to the material has been extensively studied in [13]–[15]. When a high-power laser beam is applied to a material it leads to the plasma generation of high temperature which initiates a shock wave inside the material. Eq. (6) describes the relation between the maximum applied pressure, material properties and laser parameters.

$$P_{\max} = 0.01\sqrt{\frac{\alpha}{2\alpha+3}}\sqrt{ZI_0} \tag{6}$$

where $$Z = 2\frac{Z_1 \times Z_2}{Z_1 + Z_2} \tag{7}$$

where $$Z_i = \rho_i D_i \qquad (i = 1, 2) \tag{8}$$

where $$D_i = C_0 + S \times u \qquad (i = 1, 2) \tag{9}$$

where, I_0 (GW/cm^3) is the laser's intensity, α is the part of the energy being used for the gas ionization, Z (g cm^{-2}/s^{-1}) is the material's acoustic impedance, C_0 is the sound speed inside the material, u is the material's velocity, S is a dimensionless coefficient and i is the indication factor of different materials.

The calculation of HEL values is of great importance because it describes the state 1 (Fig. 1), which is the state behind the elastic precursor. HEL values were computed using the following equations

$$t_{11}^{HEL} = \frac{\lambda_R + 2\mu_R}{2\mu_R} Y \tag{10}$$

$$\tilde{E}_{11}^{(1)} = -\frac{1}{\rho_R C_0^2} t_{11}^{HEL} \equiv -\tilde{E}_{11}^{HEL} \tag{11}$$

$$\dot{x}^{(1)} = \frac{1}{\rho_R C_0} t_{11}^{HEL} \equiv \dot{x}^{HEL} \tag{12}$$

where $\tilde{E}_{11}$ is the component of the strain tensor and $\dot{x}$ is the material's velocity. When the jump conditions are applied to the plastic wave Eqs. (13) and (14) that describe the state 2 (Fig. 1) are derived, given the stress as a boundary condition equals to $-t_{11}^{(2)} = 2.1$ GPa .

$$\tilde{E}_{11}^{(2)} = \frac{1}{\rho_R C_B^2}\left\{ t_{11}^{(2)} + \left(\frac{C_0^2 - C_B^2}{C_0^2} \right) t_{11}^{HEL} \right\} \tag{13}$$

$$\dot{x}^{(2)} = \frac{1}{\rho_R C_B}\left\{ -t_{11}^{(2)} - \left(\frac{C_0 - C_B}{C_0} \right) t_{11}^{HEL} \right\} \tag{14}$$

The state 3 (Fig. 1) is the state behind the reflected plastic compressive shock and it is characterized by the following equations

$$t_{11}^{(3)} = -\frac{C_0 + C_B}{C_0} t_{11}^{HEL} \tag{15}$$

$$\tilde{E}_{11}^{(3)} = -\frac{C_0 + C_B}{\rho_R C_0^2 C_B} t_{11}^{HEL} \tag{16}$$

$$\dot{x}^{(3)} = 0 \tag{17}$$

The interaction between the reflected plastic shock and the incident plastic shock produces the state 4 (Fig. 1) which is described by

$$t_{11}^{(4)} = t_{11}^{(2)} - \frac{C_B}{C_0} t_{11}^{HEL} \tag{18}$$

$$\tilde{E}_{11}^{(4)} = \frac{1}{\rho_R C_B^2}\left[t_{11}^{(2)} + \frac{C_0^2 - C_0 C_B - C_B^2}{C_0^2} t_{11}^{HEL} \right] \tag{19}$$

$$\dot{x}^{(4)} = \frac{1}{\rho_R C_B}\left[-t_{11}^{(2)} - t_{11}^{HEL} \right] \tag{20}$$

The final interaction inside the aluminum is the reflection of the plastic shock from the interface to a plastic compression shock that takes material from state to state 5 (Fig. 1), described by

$$t_{11}^{(5)} = 2t_{11}^{(2)} + \frac{C_0 - C_B}{C_0} t_{11}^{HEL} \tag{21}$$

$$\tilde{E}_{11}^{(5)} = \frac{1}{\rho_R C_B^2}\left[2t_{11}^{(2)} + \frac{C_B\left(C_0 - C_B\right)}{C_0^2} t_{11}^{HEL} \right] \tag{22}$$

$$\dot{x}^{(5)} = 0 \tag{23}$$

For the analytical solution, the algebraic equations were implemented into Matlab and the results will be presented in the form of Hugoniot graphs. All equations that will be used were functions of HEL values, mass density and shock wave elastic and plastic speeds. The material mechanical properties are listed in Table 1.

Parameter	**Value**
Aluminum	
Density	2700 kg/m^3
Young's Modulus	73 GPa
Poisson's ratio	0.33
Yield strength	352 MPa
Epoxy	
Density	1700 kg/m^3

Young's Modulus	4.16 GPa
Poisson's ratio	0.30
Yield strength	60 MPa

Table 1. Materials' mechanical properties [1], [2]

4 NUMERICAL MODEL

The explicit LS-DYNA software was used for the development of the FE model. Validation of the model has been done in [1], [2]. A mapped mesh consisting of different areas was developed [1], as shown in Fig. 2a. 3D 8-noded solid with one integration point elements were used. The laser's spot diameter was 4 mm (Fig. 2b). For the aluminum material the Johnson-Cook material model was used while for the epoxy an elastic plastic hydrodynamic material model used, combinedwith the Gruneisen equation of state, for both materials.

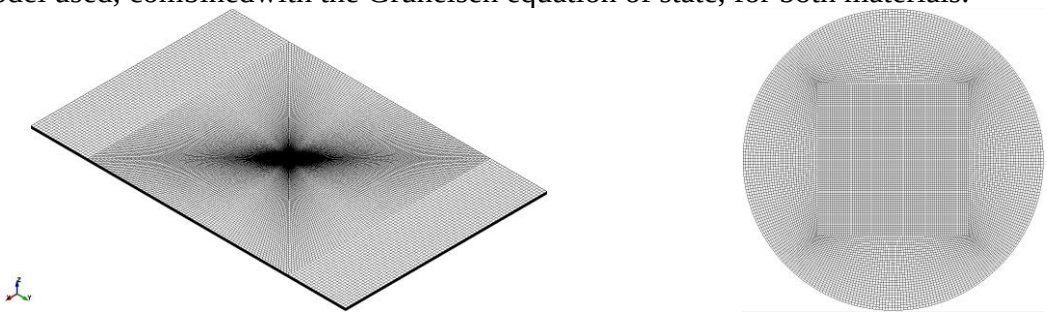

(a) (b)

Figure 2: (a) FE mesh of the specimen, (**b**) FE mesh of the circular spot [1], [2]

:5 ANALYTICAL MODELING OF SPALL FRACTURE

Spall is the process of internal failure or rupture of condensed media through a mechanism of cavitation due to stress in excess of the tensile strength of the material [4], [7]. When a threshold tensile stress is achieved, void nucleation occurs and spall fracture initiates. At relatively gentle strain rates it is suggested that the spall process involves the activation and growth of mature ductile cracks before coalescence and spall failure occurs, which is a fracture toughness-controlled phenomenon. On the contrary, at higher strain rates it is suggested that spall in the same metal is a process of hole growth and coalescence without formation of mature cracks, which is a flow stress-controlled phenomenon [7]. By an energy balance analysis [4], [7] the brittle and ductile spall strengths arise and are described by the following equations

Brittle spall strength $$P_s^B = \left(3\rho c_0 K_C^2 \dot{\varepsilon}\right)^{1/3} \tag{24}$$

Ductile spall strength $$P_s^D = \left(2\rho c_0^2 Y \varepsilon_c\right)^{1/2} \tag{25}$$

If the focus is on the epoxy the brittle spall strength must be chosen, because of the brittle nature of the epoxy material. Eq. (25) can be re-written in the following form

$$Ut \geq \frac{3\gamma}{c_0} \tag{26}$$

where $U = P^2 / 2\rho c_0^2$ is the elastic energy density, $\gamma = K_C^2 / 2\rho c_0^2$ is the fracture energy release rate and t is the time domain [7]. If we substitute U and γ in Eq. (24) and we solve for P, then Eq. (27) gives the stress threshold for the initiation of brittle spall:

$$P_{th} \geq \sqrt{\frac{6\rho c_0 \gamma}{t}} \tag{27}$$

6 RESULTS

6.1 Numerical model with CZM

Due to the lack of the exact fracture properties of the interface, calibration of the CZM is required. Since the stripping is mode-I dominated, the G_{IC} needs to be calibrated. In Fig. 3, the experimental stripping pattern is compared with the predicted stripping patterns. With blue color, the elements of the cohesive zone are presented, while with the brown color the deleted elements (stripped area) are presented. The best agreement between the test and the model is achieved for $G_{IC} = 0.95 mJ/mm^2$, which is the selected value.

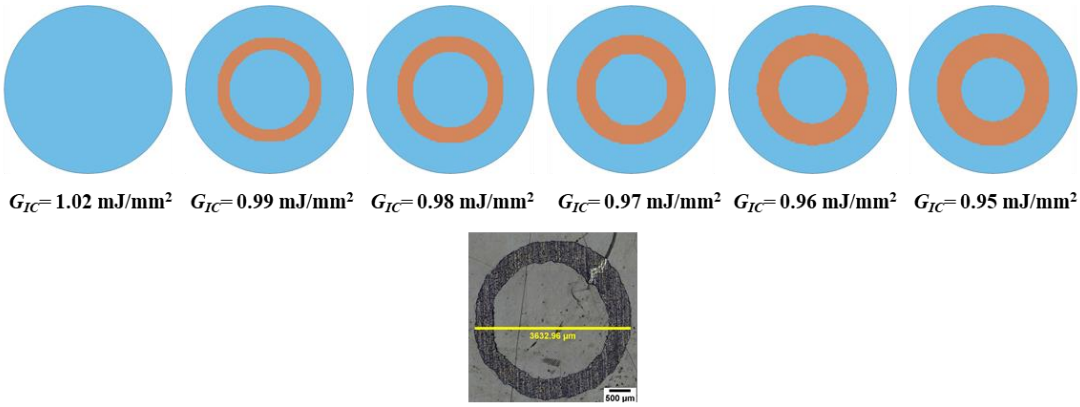

Figure 3: Comparison between experimental and numerically predicted by CZM stripping patterns for different values of G_{IC}

6.2 Analytical stress analysis

Figs. 4(a) and 4(b) plot the stress-strain and stress-velocity Hugoniots for the aluminum material, respectively. Because the interface does not accelerate [16], the stress at state 3 will be the new boundary condition of stress for the study of the shock wave that will propagate into the epoxy material. This means that the applied stress to the epoxy is at the high stress amplitude range [3]. A simple Hugoniot curve for the epoxy material is shown in Fig. 4(c) and (d). The stress of the elastic plastic decompression shock that takes the material from state 3' to state 4' and from state 5' to state 6' is $2t_{11}^{HEL} = 210$ MPa and it is of great importance because it can be compared with the interface's tensile strength or the spall fracture strength. It is noteworthy that the above applies only when the stresses are located to high stress amplitude range [3] and depends only on the mechanical properties of the material at the back free surface [6].

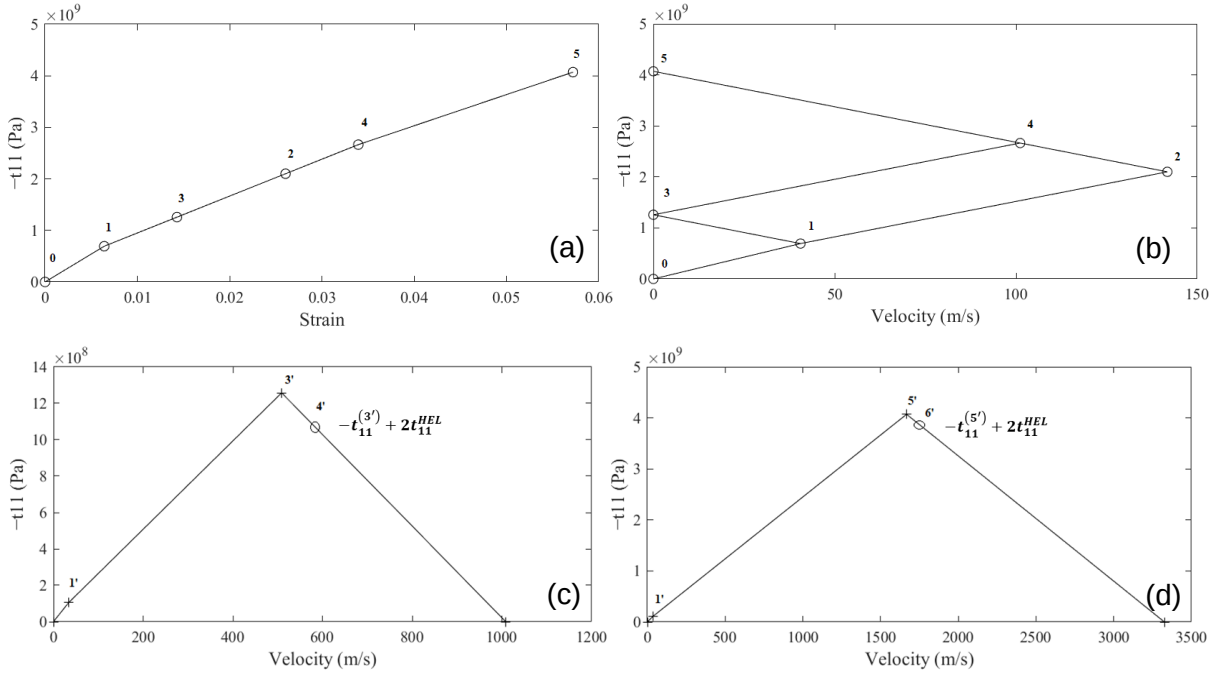

Figure 4: (a) The stress-strain Hugoniot curve, (b) The stress-material velocity Hugoniot curve, The stress-velocity Hugoniot curve for the (c) first and (d) second release wave inside epoxy

6.3 Analytical vs Numerical Stress Analysis

In this section, the tensile stresses computed by the analytical model are compared with the numerical stresses. Epoxy's yield strength and Poisson's ratio are the parameters that affecting the *HEL* values and consequently the magnitude of the tensile stress. Since the exact values of these properties are not available, for the sake of the comparison, a parametric study has been conducted. In the study, the yield strength varied from 40 to 80 MPa and the Poisson's ratio from 0.30 to 0.35. Fig. 5 compare the analytical and numerical (maximum and average) tensile stresses in the epoxy. It is shown that the yield stress of the epoxy has a greater influence on the tensile stress than the Poisson's ratio. That influence is greater for the analytical model than for the numerical model.

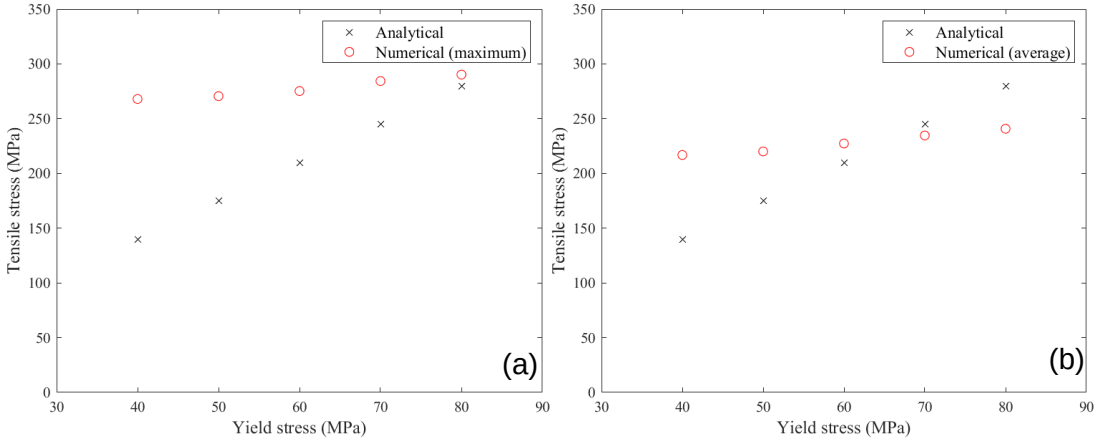

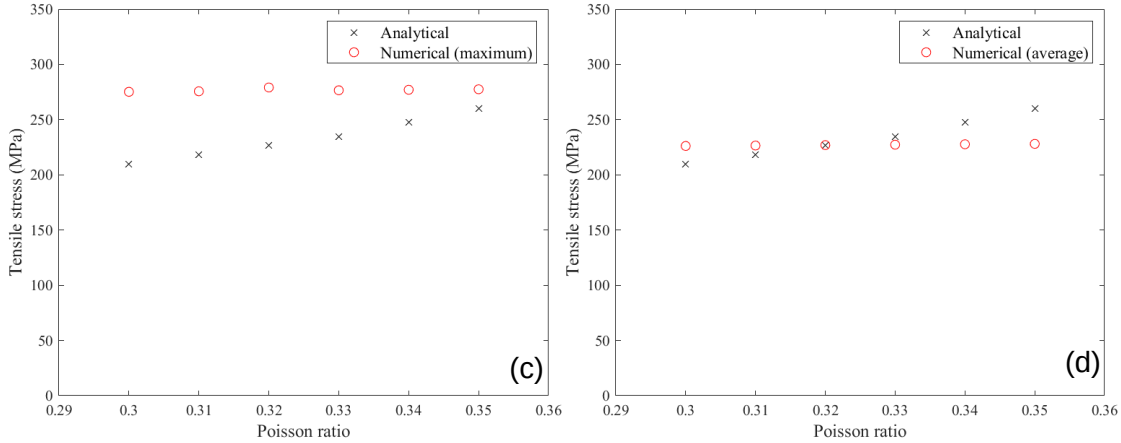

Figure 5: Variation of analytical and numerical (a) maximum and (b) average tensile stress in the epoxy with regards to the yield stress of the epoxy. Variation of analytical and numerical (c) maximum and (d) average tensile stress in the epoxy with regards to the Poisson's ratio of the epoxy

6.4 Spall fracture prediction

In this section, an approximation of the stripping stress threshold in the form of spall fracture of the aluminum/epoxy interface is presented. The methodology requires as input the fracture properties of the aluminum/epoxy interface; however, these properties could not be measured experimentally due to the difficulty in the manufacturing of the respective specimens. The authors have made many trials to manufacture double cantilever beam and end-notch flexure specimens but the curing of the thin epoxy film between the aluminum adherents was not feasible. Consequently, we have drawn the properties from the literature [16]–[18].

The stress threshold was calculated using Eq. (27). The interface's elastic modulus was derived using the following expression

$$E = \frac{K^2}{G_c} \tag{28}$$

where K is the interface's fracture toughness and G_c is the critical fracture surface energy. K was taken equal to 23.71 N·mm$^{-3/2}$, which is the average experimental value of [17]. G_c was calculated equal to 125.27 J/m^2 by (29) using the average experimental value of [17]. E was used to calculate the shock wave c speed by $c = \sqrt{E/\rho}$ for various densities ρ of the interface between 900-1100 kg/m^3. Knowing the shock wave speed at the interface and using the range of its thickness from 1 to 100 nm [18], the time domain t was then derived and used in Eq. (27) to calculate the stress threshold. γ was taken equal to 232 mJ/m^2 from [19]. Some further evaluation for interface thickness from 100 to 500 nm was made.

Fig. 6 plots the spall fracture strength for different values of the interface thickness. For small interface thickness of 1 nm, the threshold is in the range of 2.4-2.6 GPa. As the thickness increases to 20 nm, the threshold goes down to 580 MPa and for a thicker thickness of 100 nm and 500 nm it is 260 and 110 MPa, respectively. Thus, it is safe to say that the thickness plays a critical role to spall strength. On the contrary, the interface density slightly affects the spall strength.

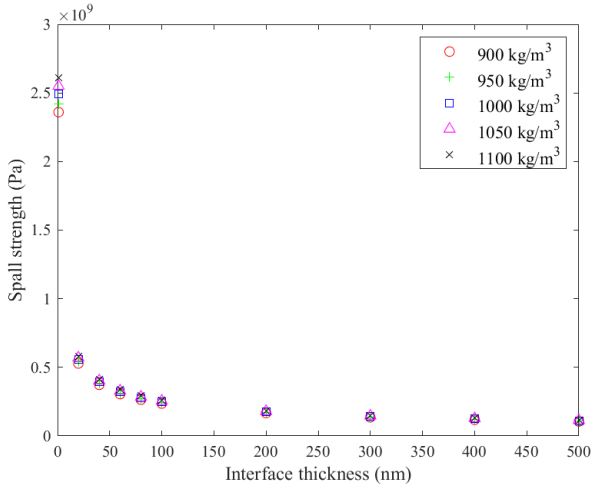

Figure 6: Variation of spall strength with the thickness of the aluminum/epoxy interface

6.5 Numerical Simulation of Stripping Using the Spall Strength

Using the spall strength values and the corresponding interface thickness in a continuum progressive damage model, taken by Fig. 6, stripping initiation and propagation can be simulated as an alternative method to CZM modeling. The interface was modeled by solid elements using the same material model and properties as the epoxy. The interface elements were eroded using an eroding parameter in MAT_000_ADD_EROSION, which is activated when the maximum principal stress of the element reaches the spall strength.

The results are illustrated in Fig. 7. For interface thickness larger than 100 nm and spall strength lower than 250 MPa, the model predicts full stripping. For lower values of interface thickness (higher values of spall strength), an annular stripping pattern is predicted. The thickness of the stripping ring decreases with decreasing the interface thickness. For interface thickness smaller than 40 nm no stripping was predicted.

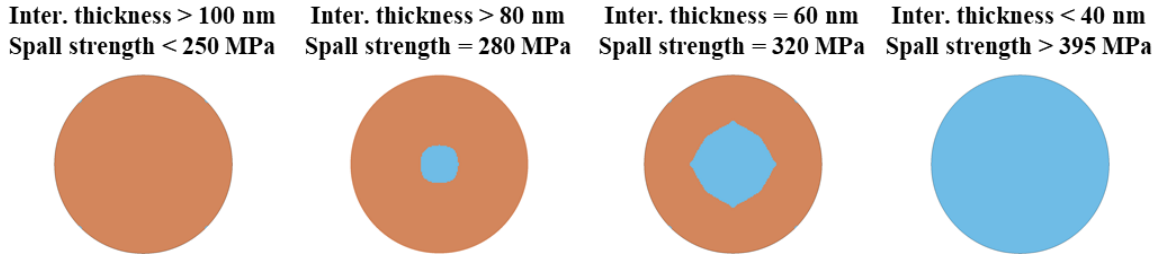

Figure 7: Stripping patterns predicted by the FE model that simulate the interface with a continuum progressive damage model based on its spall strength

6.6 Analytical prediction of stripping using spall

As a final approach, the analytical model and the spall strength model are combined to obtain a very fast prediction of stripping initiation. The analytical stress at the epoxy is compared with the spall strength of the interface based on the assumption that stress at the epoxy is close to the stress at the interface. The maximum tensile stress computed by the analytical model (210 MPa) is greater than the minimum spall strength (110 MPa) and thus, stripping is predicted using the two analytical models. Given that the numerical model predicts stripping using the spall

strength of 110–320 MPa (Fig. 6), it becomes evident that the analytical model underestimates the magnitude of the tensile stress field developed at the epoxy and the interface.

7 DISCUSSION AND CONCLUSIONS

In the present study we have developed analytical and numerical models to compute the stress field and predict the failure of an aluminum/epoxy interface subjected to laser shock loading in the frame of the paint stripping technological problem. The FE model with the CZM is the most accurate tool, although in most cases it is the most computationally expensive. The spall fracture model has given trusted estimations of the spall strength of the interface which are very sensitive to the interface thickness and less sensitive to the interface density. The analytical stress analysis model can be used to efficiently represent the shock wave propagation into the material system, but it can give only a preliminary estimation of the tensile stress at the epoxy, which is very sensitive to the yield stress and Poisson's ratio of the epoxy. In Fig. 8 a qualitative comparison of the different approaches in terms of required time, accuracy, and input properties is presented.

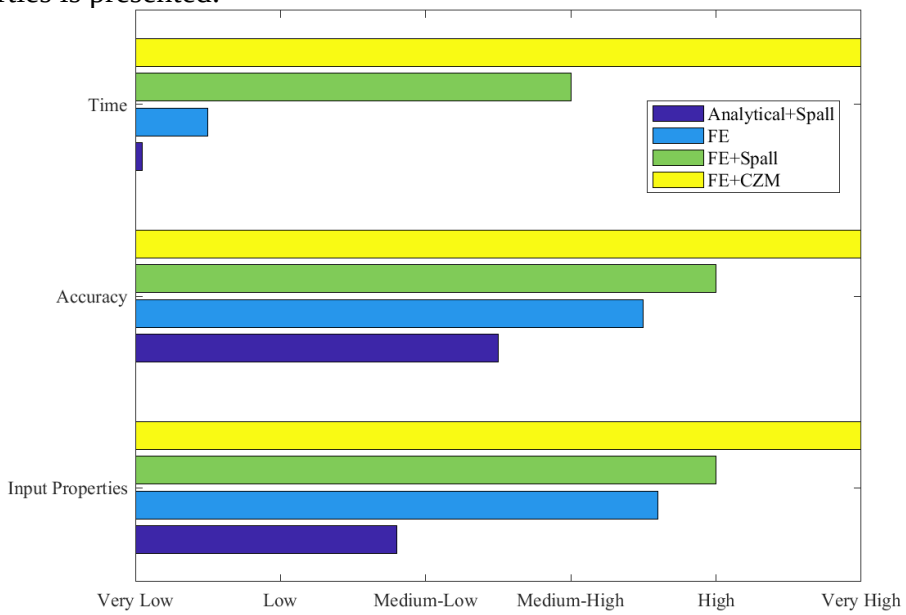

Figure 8: Qualitative comparison of the different models that predict spallation of the interface

REFERENCES

[1] S. Ünaldi *et al.*, "Towards selective laser paint stripping using shock waves produced by laser-plasma interaction for aeronautical applications on AA 2024 based substrates," *Optics & Laser Technology*, vol. 141, p. 107095, Sep. 2021, doi: 10.1016/j.optlastec.2021.107095.

[2] K. Tserpes, K. Papadopoulos, S. Unaldi, and L. Berthe, "Development of a Numerical Model to Simulate Laser-Shock Paint Stripping on Aluminum Substrates," *Aerospace*, vol. 8, no. 9, p. 233, Aug. 2021, doi: 10.3390/aerospace8090233.

[3] L. Davison, *Fundamentals of Shock Wave Propagation in Solids*. Berlin, Heidelberg: Springer Berlin Heidelberg, 2008. doi: 10.1007/978-3-540-74569-3.

[4] D. E. Grady, *Physics of shock and impact. Volume 1, Fundamentals and dynamic failure*. 2017.

[5] D. E. Grady and Institute of Physics, *Physics of shock and impact, Volume 2, Materials and shock response*. 2017.
[6] L. Lapostolle, K. Derrien, L. Morin, L. Berthe, and O. Castelnau, "Modeling and simulation of laser shock waves in elasto-plastic 1D layered specimens," *International Journal of Solids and Structures*, vol. 239–240, p. 111422, Mar. 2022, doi: 10.1016/j.ijsolstr.2022.111422.
[7] D. E. Grady, "The spall strength of condensed matter," *Journal of the Mechanics and Physics of Solids*, vol. 36, no. 3, pp. 353–384, Jan. 1988, doi: 10.1016/0022-5096(88)90015-4.
[8] G. I. Kanel, V. E. Fortov, and S. V. Razorenov, *Shock-Wave Phenomena and the Properties of Condensed Matter*. 2004. Accessed: Apr. 01, 2022. [Online]. Available: https://doi.org/10.1007/978-1-4757-4282-4
[9] A. Tarabay, D. Curran, S. Razorenov, L. Seaman, G. Kanel, and A. Utkin, *Spall fracture*. New York: Springer, 2003.
[10] R. Ecault, F. Touchard, M. Boustie, L. Berthe, and N. Dominguez, "Numerical modeling of laser-induced shock experiments for the development of the adhesion test for bonded composite materials," *Composite Structures*, vol. 152, pp. 382–394, Sep. 2016, doi: 10.1016/j.compstruct.2016.05.032.
[11] C. Le Bras *et al.*, "Laser Shock Peening: Toward the Use of Pliable Solid Polymers for Confinement," *Metals*, vol. 9, no. 7, p. 793, Jul. 2019, doi: 10.3390/met9070793.
[12] K. Papadopoulos and K. Tserpes, "Analytical and Numerical Modeling of Stress Field and Fracture in Aluminum/Epoxy Interface Subjected to Laser Shock Wave: Application to Paint Stripping," *Materials*, vol. 15, no. 10, p. 3423, May 2022, doi: 10.3390/ma15103423.
[13] L. Berthe, R. Fabbro, P. Peyre, L. Tollier, and E. Bartnicki, "Shock waves from a water-confined laser-generated plasma," *Journal of Applied Physics*, vol. 82, no. 6, pp. 2826–2832, Sep. 1997, doi: 10.1063/1.366113.
[14] R. Fabbro, P. Peyre, L. Berthe, and X. Scherpereel, "Physics and applications of laser-shock processing," *Journal of Laser Applications*, vol. 10, no. 6, pp. 265–279, Dec. 1998, doi: 10.2351/1.521861.
[15] R. Fabbro, J. Fournier, P. Ballard, D. Devaux, and J. Virmont, "Physical study of laser-produced plasma in confined geometry," *Journal of Applied Physics*, vol. 68, no. 2, pp. 775–784, Jul. 1990, doi: 10.1063/1.346783.
[16] O. A. Hurricane and P. L. Miller, "Shock transmission and reflection from a material interface and subsequent reflection from a hard boundary," UCRL-ID-132586, 6132, Nov. 1998. doi: 10.2172/6132.
[17] Chul Jin Syn and W. W. Chen, "Surface Morphology Effects on High-Rate Fracture of an Aluminum/Epoxy Interface," *Journal of Composite Materials*, vol. 42, no. 16, pp. 1639–1658, Aug. 2008, doi: 10.1177/0021998308092212.
[18] F. Cavezza, M. Boehm, H. Terryn, and T. Hauffman, "A Review on Adhesively Bonded Aluminium Joints in the Automotive Industry," *Metals*, vol. 10, no. 6, p. 730, Jun. 2020, doi: 10.3390/met10060730.
[19] L. F. M. da Silva, A. Öchsner, and R. D. Adams, Eds., *Handbook of Adhesion Technology*. Berlin, Heidelberg: Springer Berlin Heidelberg, 2011. doi: 10.1007/978-3-642-01169-6.